

The architecture of active zone material at the frog's neuromuscular junction

Mark L. Harlow, David Ress, Arne Stoschek, Robert M. Marshall & Uel J. McMahan

Department of Neurobiology, Stanford University School of Medicine, Stanford, California 94305, USA

Active zone material at the nervous system's synapses is situated next to synaptic vesicles that are docked at the presynaptic plasma membrane, and calcium channels that are anchored in the membrane. Here we use electron microscope tomography to show the arrangement and associations of structural components of this compact organelle at a model synapse, the frog's neuromuscular junction. Our findings indicate that the active zone material helps to dock the vesicles and anchor the channels, and that its architecture provides both a particular spatial relationship and a structural linkage between them. The structural linkage may include proteins that mediate the calcium-triggered exocytosis of neurotransmitter by the synaptic vesicles during synaptic transmission.

At synapses throughout the nervous system, one or more areas on the cytoplasmic surface of the plasma membrane of presynaptic nerve cells are studded with distinctive aggregates of proteins. The aggregates can only be observed by electron microscopy (EM), and they are viewed best in sections from fixed, plastic-embedded tissue, where they stain with heavy metals¹. They are confined to the portion of the presynaptic membrane that faces the narrow cleft between the pre- and postsynaptic cell, and some of the presynaptic cell's numerous synaptic vesicles, which contain neurotransmitter molecules, are docked on (that is, held at) the membrane next to them. When an electrical impulse in the presynaptic nerve cell arrives at the synapse, it causes calcium channels in the presynaptic membrane near to the protein aggregates to open, thereby permitting calcium ions to enter the cell. The influx of calcium triggers events that cause the membrane of the docked vesicles to fuse with the presynaptic membrane, and the subsequent exocytosis of the neurotransmitter into the synaptic cleft^{2–4}. Thus, the protein aggregates are situated at the active zones of the presynaptic membrane, the sites where initial events in the rapid neurotransmitter-mediated signalling between the pre- and postsynaptic cells take place. Since their detection⁵, the protein aggregates have been referred to in a variety of ways including membrane thickenings and presynaptic dense projections as well as active zone material (AZM), the term we use here.

The proximity of AZM to docked synaptic vesicles and calcium channels suggests that it is physically connected to one or both structures, and raises questions about the possible function of such connections^{6–8}. We used electron microscope tomography (EMT) to examine the structure and associations of AZM in tissue sections from neuromuscular junctions. Transmission EM provides two-dimensional projections of specimens, which are captured on film or CCD (charge-coupled device). Conventionally, data analysis is done on these projections, but the level of detail is restricted by the absence of depth information. In particular, components of the AZM are indistinct and their relationships are uncertain even in the thinnest sections that can be routinely cut (30–50 nm). Electron microscope tomography, which has been developed mostly over the last decade, provides three-dimensional reconstructions of specimens by using a series of two-dimensional projections made at different tilt angles⁹. The increased spatial resolution obtained from three-dimensional reconstructions over two-dimensional projections—more than an order of magnitude along the *z*-axis—has already been useful for markedly enhancing understanding of certain macromolecules, viruses and cellular organelles in *in vitro* preparations^{10–14}. It has also been used for determining in stained tissue sections the shapes and relationships of subcellular structures

that have a high signal/noise ratio and a simple geometry^{15–18}. Because the components of AZM have a complex configuration and are of moderate to low contrast in tissue sections, we found it necessary to combine advanced image restoration and new three-dimensional segmentation methods for our analysis. We provide a detailed account of the organization and connections of AZM, and a refined hypothesis as to its function.

Overviews

Conventional two-dimensional EM has shown that each patch of AZM at the frog's neuromuscular junction is elongate, with its long axis lying parallel to the presynaptic membrane^{3,19} (Fig. 1a, b). It is frequently 1–2 μm long and about 75 nm wide, extending 50–75 nm from the presynaptic membrane into the terminal's cytoplasm. On each flank there is a row of docked vesicles, and where the AZM is adjacent to the presynaptic membrane, the membrane curves outward forming a 'ridge'¹⁹. On each slope of the ridge, as seen by EM on replicas of freeze-fractured specimens, the membrane contains a linear array of macromolecules that parallels the long axis of the AZM. The array may include multiple species of proteins, but evidence indicates that the proteins that form calcium channels are concentrated within it^{20–22}. Thus, at this synapse, the calcium channels are apparently concentrated in two specific portions of the presynaptic membrane directly beneath the AZM, each portion parallel and close to one of the rows of docked vesicles flanking the material (Fig. 1a, b).

Figure 1c is a two-dimensional EM image of an active zone in a 50-nm-thick tissue section from a frog's neuromuscular junction. It is similar to the images used for the scheme in Fig. 1a, b. It is also the 0° image of a data set of two-dimensional tilt images, called MPI-10, that we used to reconstruct the section's volume. The plane of the section is nearly transverse to the AZM. The AZM is flanked by docked vesicles, and its superficial surface follows the contour of the presynaptic membrane where it forms the active zone ridge. Components of the AZM are evident, but their size, shape and relationships are indeterminate because of the absence of depth information.

There is no uncertainty, however, about the components of AZM in two-dimensional images of 0.5-nm (2 voxel) slices through the reconstructed volumes from MPI-10 and from another active zone, MPI-9 (Fig. 1d, e). Individual components are spatially resolved in three dimensions, so that their size, shape and associations can be determined accurately. Serial slices through the entire volume of the active zones revealed that the components were generally elongate. One end of some components was continuous with the membrane of the docked vesicles. In such cases, the otherwise nearly smooth

curvature of the vesicle membrane was distorted toward the components (Fig. 1d, e). These distortions would be expected if the components were connected to the vesicles, and the connections had withstood some tension generated either *in vivo* or during preparation for microscopy.

A more coherent perspective of the AZM, synaptic vesicles and presynaptic membrane in MPI-10 and MPI-9 was obtained by segmenting and surface-rendering these structures. The three-dimensional views showed that much of the four docked vesicles had been included in the tissue sections (Fig. 1f–i). They also showed that the AZM was widely distributed over the slopes of the active zone ridge, that it formed many connections with each vesicle, and that the components were, in general, interconnected.

Connections to docked synaptic vesicles

Examination of the serial volume slices from MPI-9 and MPI-10 show that the number of components connected to the four partial vesicles ranged from seven to twelve, with each component forming only one connection. In two cases, two components seemed to be conjoined at their sites of connection to the vesicles, but in all other cases the components contacted the vesicles separately. We used surface renderings to examine the distribution of connection sites between the vesicles and AZM. To expose the connections, we made partial segmentations that included only the short portions (~1 nm) of the components where they contacted the vesicles (Fig. 2a–d). Connection sites were widely distributed on the half of the vesicles facing the AZM. Several connections were 10–15 nm

from the vesicle–presynaptic membrane interface, where vesicle fusion with the presynaptic membrane takes place during synaptic transmission. Cytoplasmic structures other than those comprising the AZM also were in contact with docked vesicles in MPI-9 and MPI-10 (Fig. 1f–i). However, there were only three or four such contacts per vesicle, and they were primarily on the half of the vesicles that faced away from the AZM.

Beams and ribs

To determine whether any of the components that contacted the docked synaptic vesicles near the vesicle–presynaptic membrane interface were also associated with the macromolecule-containing regions of the presynaptic membrane along the slopes of the active zone ridge, we undertook a detailed examination of the architecture of the AZM within 15 nm of the membrane.

All of the components in the first 15 nm of AZM in MPI-10 and MPI-9 were elongate (Figs 3a–d and 4a). We initially identified two types on the basis of their position and orientation, which we call beams and ribs. The beams lay near the midline of the presynaptic ridge, nearly parallel to the ridge’s long axis. Ribs extended along the slopes of the ridge, nearly orthogonal to its long axis. In MPI-10, six of the seven ribs contacted the synaptic vesicles near the vesicle–presynaptic membrane interface (Figs 3c and 4a), and they accounted for all of the contacts made by AZM at the interface (Fig. 2a, b). The one rib that did not contact a vesicle was at the surface of the section, and may have contacted a vesicle that was not included in the section. Nearly all of the ribs from both slopes of the

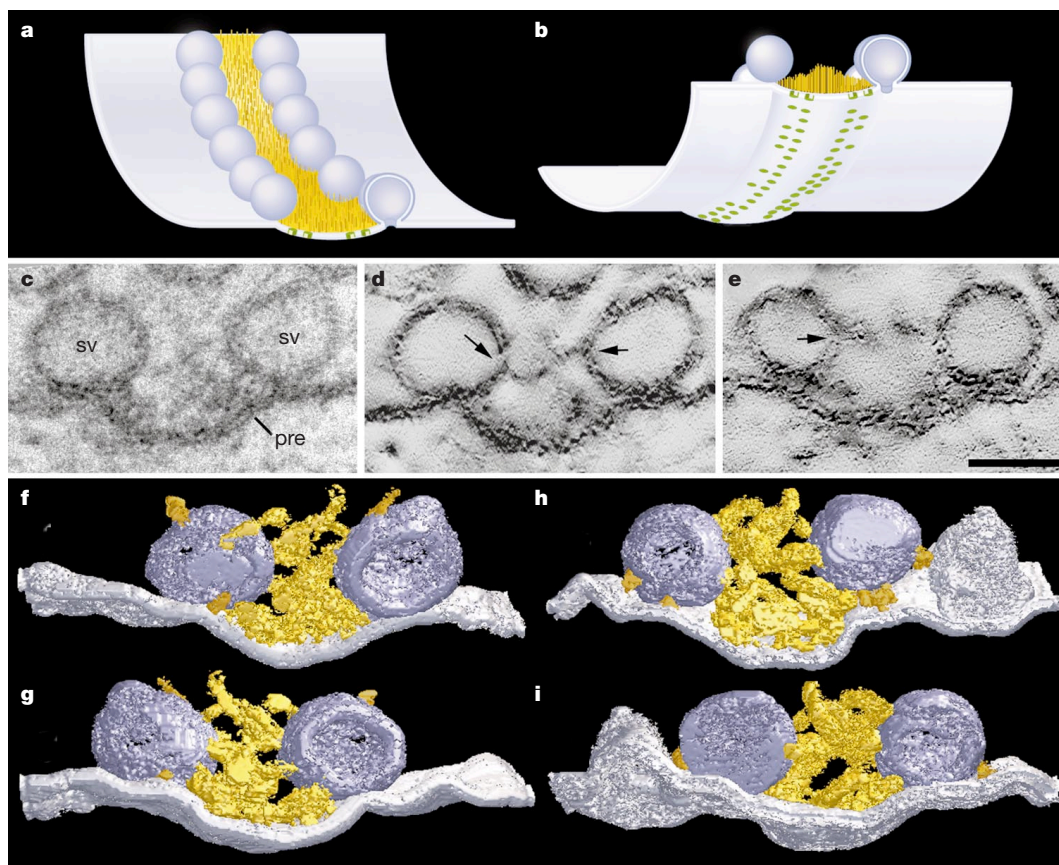


Figure 1 Two-dimensional and three-dimensional (2D and 3D, respectively) overviews. **a, b**, Schematized relationships of AZM based on conventional 2D EM. The colour code for AZM (gold), docked synaptic vesicles (dark blue), presynaptic membrane with active zone ridge (pale blue) and macromolecules along the slopes of the ridge (green) are the same in all figures, except where indicated. **c**, The 0° image of MPI-10 from a tissue section. AZM is indicated by an arrow. sv, docked synaptic vesicles; pre, presynaptic membrane. **d, e**, 0.5-nm volume slices from the reconstruction of MPI-10 (**d**) and MPI-9 (**e**). The smooth

curvature of the vesicles is distorted at the sites of contact (arrows) between AZM and vesicles, indicative of tension. Scale bar, 50 nm (**c–e**). **f–i**, 3D views of segmented, surface-rendered AZM, docked vesicles and presynaptic membrane in MPI-10 (**f**, front; **g**, back) and MPI-9 (**h**, front; **i**, back). The hummock in the presynaptic membrane in **h** and **i** is a vesicle of unknown type that is undergoing either exo- or endocytosis. Cytoplasmic structures associated with the synaptic vesicles but not part of the AZM are bronze.

ridge in MPI-10 also terminated on a single beam (Fig. 3c). In the two exceptions, ribs from opposite slopes terminated on a short structure at the surface of the section, which was probably part of a beam that was not fully included in the section. In MPI-9, seven of the eight ribs contacted a beam (Fig. 3d): the exception was interrupted near the beam. The plane of the tissue section for MPI-9 was intermediate to the transverse and horizontal planes of the AZM, so that the lateral portions of some of the ribs were not included in the section. However, each of the four ribs that could be traced to their lateral ends contacted a vesicle near the vesicle–presynaptic membrane interface (Fig. 3d), and these contacts accounted for all of the contacts made by AZM at the interface (Fig. 2c, d). Thus, for both MPI-9 and MPI-10, all of the components of AZM that contacted vesicles near the vesicle–presynaptic membrane interface were ribs, all ribs lay in close apposition to the presynaptic membrane along the slopes of the active zone ridge, and nearly all of the ribs were connected to a beam.

We observed many more ribs and beams in the first 15 nm of AZM in another tissue section that we reconstructed from data set UC-1. The tissue section was cut nearly parallel to the horizontal plane of the AZM, so that more of the active zone was included than in the sections used for MPI-9 and MPI-10, and data were collected at a lower magnification. Thirteen docked vesicles were associated with forty ribs that were nearly parallel to one another and orthogonal to the long axis of the active zone ridge (Fig. 3e, f). Seven beams lay parallel to the long axis of the ridge near its midline. Five beams were in series and two were paired, with the ends of adjacent ones overlapping and contacting one another (Fig. 3e–g). One end of all the ribs contacted a vesicle (Fig. 3f), and the other end of most ribs contacted a beam (Fig. 3e, f). For the exceptions, the gaps between the ribs and beams were of various lengths. Thus, the arrangement and the connectivity of ribs and beams in the relatively long stretch of AZM provided by UC-1 were the same as in MPI-9 and MPI-10.

We found the following characteristics of ribs and beams: those ribs terminating on each of the paired beams in UC-1 were shorter

than those terminating on the serial beams (Fig. 3e, f). This shows that ribs can have different lengths. In most cases, the ribs tapered as they approached their contact points with beams (Fig 3). They also tapered as they approached their contact points with synaptic vesicles, but more acutely (data not shown). Indeed, the general thickness of the ribs was usually greatest where they were adjacent to the region of the presynaptic membrane that contained the linear array of macromolecules. Of the ten beams we observed in MPI-9, MPI-10 and UC-1, we could be certain of only two having their full length included in the samples (Fig. 3g). Both were ~75 nm long; although some of the uncertain beams were as long as these two ~75-nm beams, none were longer.

To learn whether there was a correlation between the frequency of the ribs along the active zone ridge and the frequency of macromolecules in the adjacent presynaptic membrane, we compared our images of rib–beam assemblies with images of the macromolecules in replicas from freeze-fractured neuromuscular junctions of the frog. The linear array of macromolecules on each slope of an active zone ridge in a previously published image⁴ is shown in Fig. 3h. Each array is an often-interrupted string of conspicuously large particles that have a nearly regular spacing characterized by a longitudinal frequency. The particles occur singly or in pairs, the latter characterized by a transverse frequency. The same image of the replica, overlaid with images of surface-rendered rib–beam assemblies from UC-1, shows a strong similarity between the longitudinal frequency of the particles and the frequency of ribs (Fig. 3i). We tested this correlation by determining the mean centre-to-centre spacing of continuous runs of particles (1,100 measurements; only one member of paired particles was included) in replicas²³ from five freeze-fractured neuromuscular junctions and comparing it with the mean midline-to-midline spacing of the ribs in the rib–beam assemblies from MPI-9, MPI-10 and UC-1 (45 measurements on surface renderings at points where the ribs overlay the slopes of the active zone ridge). The muscles were fixed with glutaraldehyde, and were taken from frogs of the same age and size as those used for tomography (see Methods). The spacing of the particles/macromolecules (17.2 ± 3.6 nm) was in good agreement with the spacing of the ribs (16.1 ± 3.4 nm).

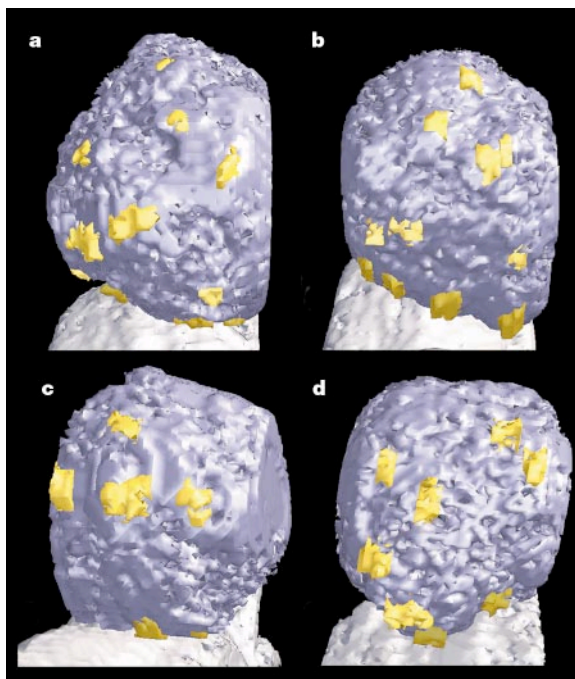


Figure 2 Sites of connections between components of AZM and docked vesicles. **a–d**, Median view of docked vesicles in MPI-10 (**a, b**) and MPI-9 (**c, d**) together with short portions of components (light and dark gold) marking the connections. The portions nearest to the presynaptic membrane (dark gold) are the ends of ribs.

Pegs

Examination of the serial volume slices from the reconstructions of MPI-9 and MPI-10 showed that the ribs were separated from the presynaptic membrane by a narrow gap (≤ 7 nm). At intervals, components of AZM extended across the gap, connecting the ribs to the regions of the membrane containing the macromolecules (Fig. 4a). We have called these components pegs. Segmentations of rib–beam assemblies in MPI-9 and MPI-10, together with a portion (~1 nm) of each peg where it connected to a rib, showed that each rib had one or two such connections (Fig. 4b, c). Segmentation of the presynaptic membrane in MPI-9 and MPI-10, together with a portion of each peg where it connected to the membrane, showed that the longitudinal and transverse frequencies of the peg–membrane connections along the active zone ridge were markedly similar to the longitudinal and transverse frequencies of the macromolecules in freeze-fracture replicas (Fig. 4d–f). Cytoplasmic proteins generally connect to membranes by binding to the membranes’ proteins. Because the only discernible membrane proteins on the slopes of the active zone ridge that had a distribution similar to that of the pegs were the macromolecules, our findings indicate that all ribs are connected by means of pegs to most, if not all, of the macromolecules in the presynaptic membrane, and that each rib is so connected to at least one or two macromolecules.

Refined and extended hypothesis

Our study shows that the AZM at the frog’s neuromuscular junction consists of elongate, interconnected components, and that some of these components are also connected to synaptic vesicles docked at

the presynaptic membrane. The fact that each docked vesicle included in our samples was connected to many components provides strong evidence that the AZM, as previously suggested⁶, is involved directly in vesicle docking. We also show that some components of the AZM are connected selectively to the narrow regions of presynaptic membrane that contain a linear array of macromolecules, which includes calcium channels, and we provide evidence that most, if not all, of the macromolecules have such connections. Proteins clustered in the postsynaptic membrane of muscle fibres and in the plasma membrane of other cell types are known to be anchored to cytoplasmic proteins, which inhibit their lateral mobility²⁴. Accordingly, it is probable that components of the AZM that are linked to the macromolecules in the presynaptic membrane contain proteins that help to anchor calcium channels and any other membrane proteins that may also be in the linear

arrays^{25,26}.

Our detailed examination of AZM that lay within 15 nm of the presynaptic membrane revealed that the components have a highly ordered distribution, with there being three topologically distinct types: ribs, beams and pegs. In most cases, these three components were interconnected in a systematic way, and this assembly had specific connections to docked synaptic vesicles and regions of the presynaptic membrane that contained the macromolecules. In the few cases where there were gaps in and between components that were not apparent elsewhere, it is probable that such gaps were the result of our inability to adequately fix or stain the components during preparation for microscopy. Thus, we propose (Fig. 5) that for the first 15 nm of AZM at resting neuromuscular junctions, the typical architecture consists of beams that are linked to each other and to ribs, ribs linked to

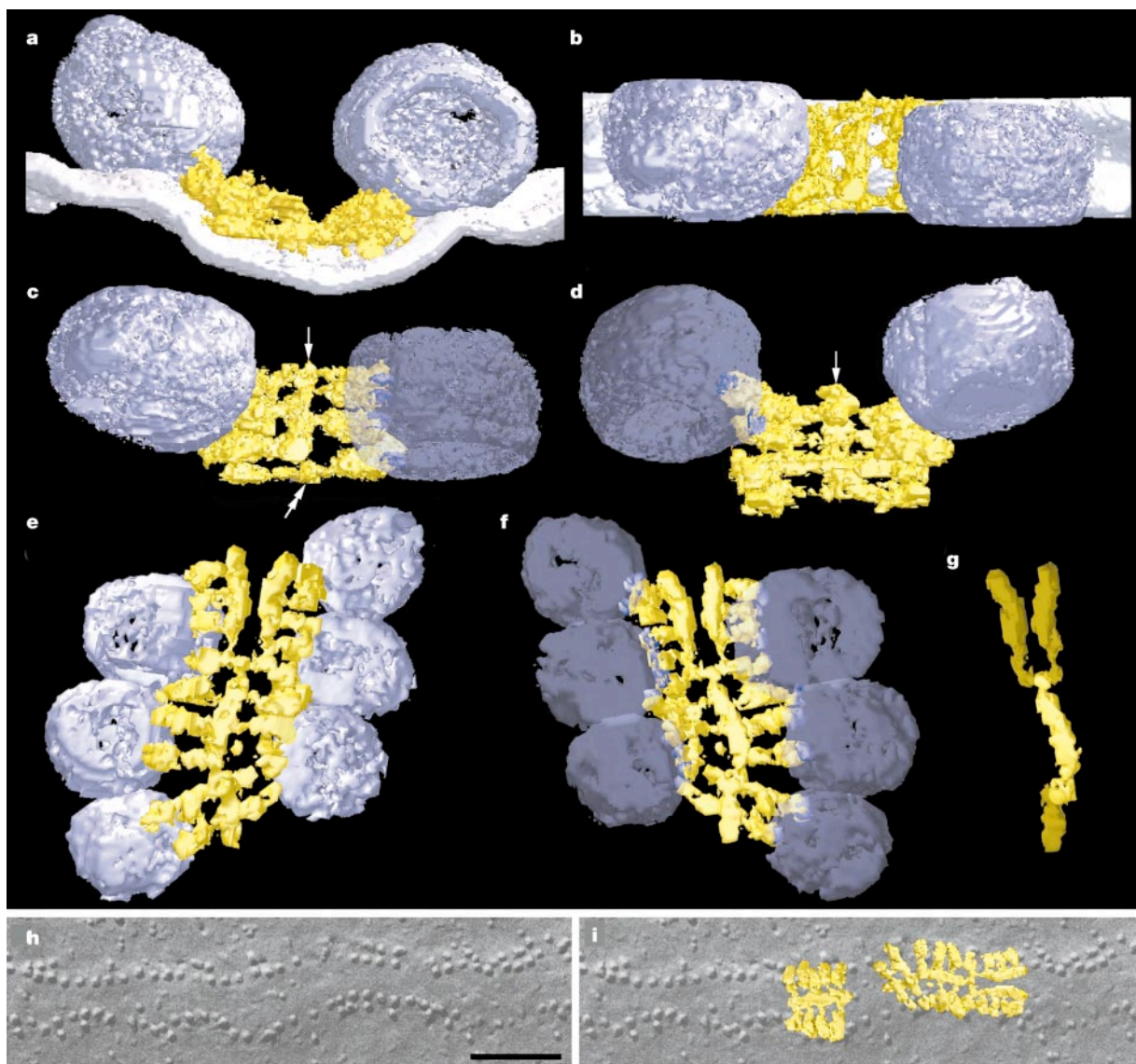


Figure 3 Distribution and associations of ribs and beams. **a, b**, Transverse and horizontal views, respectively, of the first 15 nm of AZM internal to the presynaptic membrane in MPI-10, together with the membrane and docked vesicles. **c**, View similar to that in **b** with the presynaptic membrane removed. We have made one vesicle transparent to show four complete ribs. Contact sites of these ribs with the transparent vesicle are indicated as bright blue patches. Most of the ribs contact the same beam (arrow), and two contact another beam (double arrow). **d**, View of ribs and a beam (arrow) in MPI-9, similar to that shown for MPI-10 in **c**. **e–g**, Horizontal views from the presynaptic membrane (**e**), and from the cytoplasm (**f, g**) of the first 15 nm of AZM and docked vesicles from a portion of

the reconstructed volume in UC-1. Numerous ribs extend between vesicles and beams (**e**). We have made the vesicles transparent to show points of rib–vesicle contact (bright blue) (**f**); only the beams are shown in **g**. One beam (light gold) can be traced to connections to other ribs at both of its ends. **h**, Replica⁴ from a freeze-fractured frog's neuromuscular junction showing a series of particles/macromolecules on each slope of a ridge. Scale bar, 100 nm. **i**, Same replica with surface-rendered rib–beam assemblies from UC-1 superimposed at the same scale as the replica, which shows the similarity in longitudinal frequency between ribs and macromolecules. (See Supplementary Information for movies.)

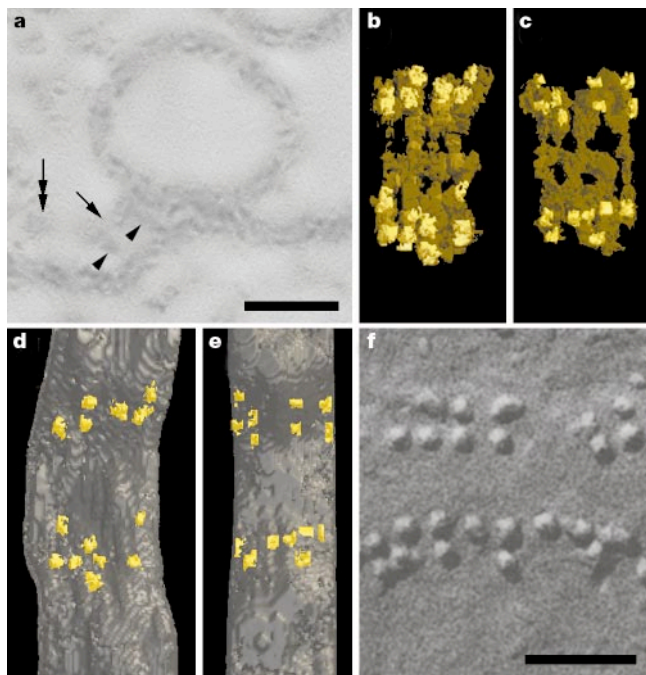


Figure 4 Arrangement and relationships of pegs. **a**, 2D projection of a 2.5-nm volume slice from MPI-10, transverse to the AZM, showing a rib (arrow) extending from a synaptic vesicle toward a beam (double arrow). Two pegs (arrowheads) extend from the rib to the presynaptic membrane. Scale bar, 25 nm. **b, c**, Horizontal views of surface-rendered rib-beam assemblies (dark gold) in MPI-10 and MPI-9, respectively, that also include short portions of pegs (light gold) marking the sites where the pegs contact the ribs. **d, e**, Horizontal views of surface-rendered presynaptic membranes in MPI-10 and MPI-9, respectively, that also include short portions of pegs (gold) marking the sites where the pegs contact the membranes. **f**, Portion of the replica of freeze-fractured presynaptic membrane shown in Fig. 3h that is scaled for comparing the longitudinal and transverse frequencies of macromolecules in the membrane to the longitudinal and transverse frequencies of peg-membrane contacts in **d** and **e**. Scale bar, 50 nm.

docked vesicles and pegs, and pegs linked to the macromolecules in the presynaptic membrane. This leads to the broader hypothesis that the assembly of ribs, beams and pegs, augmented by the remainder of the AZM, acts as a scaffold that helps to maintain the linear arrangement of, and spacing between, docked vesicles and the macromolecules.

At least some of the pegs and ribs may be involved directly in regulating the fusion of docked vesicles with the presynaptic membrane during synaptic transmission. On the basis of the amount of the calcium channel protein that is cytoplasmic²², each channel may make up part or all of a peg, and even extend into part of a rib. Ribs may also contain proteins that mediate the effects of calcium on vesicle fusion. Evidence indicates that the cytoplasmic domains of certain proteins in the membrane of docked vesicles are bound to the cytoplasmic domains of certain other proteins in the presynaptic membrane, and the association of these so-called SNARE proteins brings the vesicles and presynaptic membrane into direct apposition^{27,28}, perhaps into partial fusion²⁹. Moreover, the cytoplasmic domains of one of the presynaptic membrane's SNARE proteins, syntaxin, and another vesicle protein, synaptotagmin, may be linked to the calcium channels²², and the SNAREs and synaptotagmin may help mediate the calcium-triggered fusion of docked vesicles with the presynaptic membrane, thereby leading to the exocytosis of neurotransmitter during synaptic transmission^{28–30}. If the cytoplasmic domains of syntaxin and synaptotagmin are linked to the calcium channels at the frog's neuromuscular junction, they must pass through the AZM to reach the channels. Our observation that the ribs contact vesicles near the site where the

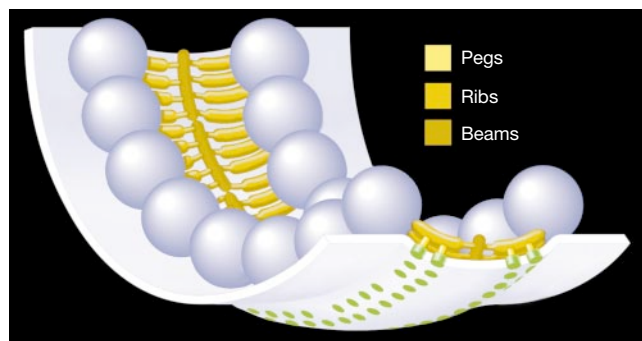


Figure 5 Arrangement and connections of pegs, ribs and beams.

vesicles are in close apposition to the presynaptic membrane raises the possibility that syntaxin and synaptotagmin reach the calcium channels through the ribs. The involvement of ribs in the fusion of vesicles with the presynaptic membrane would distinguish them from other AZM components connected to the vesicles, which may simply recognize and tether^{31,41} the vesicles.

In sum, we propose that the AZM is a multifunctional organelle that regulates the docking and fusion of synaptic vesicles at, and with, the presynaptic membrane, the anchoring of calcium channels in the membrane and the maintenance of spatial relationships between docked vesicles and channels. The material is also likely to be involved in the adhesion of the pre- to the postsynaptic membrane through the extracellular matrix^{5,32–34}. Electron microscope tomography studies aimed at determining how ribs and beams are associated with deeper components of the AZM, and how the material is associated with cytoplasmic components that mediate vesicle transport to the active zone, may indicate additional functions. Our general hypothesis should be testable at neuromuscular junctions and other synapses by combining EMT with well-established procedures for localizing specific proteins, and for studying the behaviour of synaptic organelles during synaptic transmission. Accurate information about the three-dimensional structural organization of the AZM and the molecular nature of its components is essential for a complete understanding of the presynaptic mechanisms that are involved in the regulation of synaptic transmission throughout the nervous system. □

Methods

Sample preparation

We used a conventional procedure^{23,35}. Briefly, cutaneous pectoris muscles of adult *Rana pipiens* (5 cm nose–rump length) were, in sequence, fixed with 1% phosphate buffered glutaraldehyde, refixed and stained with 1% osmium tetroxide in phosphate buffer, stained with saturated aqueous uranyl acetate, dehydrated in ethanol and propylene oxide, and embedded in Epon 812. Thin sections that had a silver interference colour (~50 nm thick) were mounted on 1 × 2 mm single slot Formvar coated grids, and stained with uranyl acetate, followed by lead citrate. For use in the alignment of tilt images, stained and mounted sections were floated on a drop of ~0.01% unconjugated gold colloid in H₂O (Sigma Chemical, St Louis, Missouri) for 1–2 min, and air dried.

Data collection

Data sets for MPI-9 and MPI-10 were made with a Philips CM200 electron microscope operated at 120 kV and equipped with a FEG, LN₂ cryoholder (Gatan, Warrendale, Pennsylvania) and 1024 × 1024 CCD (Tietz Video and Image Processing Systems GmbH, Gauting, Germany). The images were made on the CCD camera at a magnification of ×69,700, giving a single pixel size of 0.26 nm in the image. The tilt series was collected using an automatic procedure^{36,37}. Sections were pre-irradiated for 0.5–1.5 min, which, together with their low temperature, reduced shrinkage during data collection³⁸. For MPI-9, the tilt series consisted of 64 images spanning angles from –66° to +60° in 2° increments. For MPI-10, the series consisted of 67 images spanning angles from –62° to +70° in 2° increments. We made the data set for UC-1 on a Philips EM 430 electron microscope that was equipped for automatically collecting serial tilt images and was operated at 300 kV. It had a LaB₆ electron source, a cryoholder and a 1024 × 1024 CCD. The tilt series consisted of 140 images spanning angles from –70° to +69° in 1° increments. The images were made on the CCD camera at a magnification of ×30,600 with a bin size of two, so that the pixel size was 1.2 nm in the image.

Tomographic reconstruction

The gold beads on a section served as markers for aligning the tilt images. We used a scheme³⁵ that automatically detected the position of these markers and indexed them from image to image. The resulting set of position vectors was then arranged in a matrix representation of the tilt geometry, and the alignment information was obtained by inversion. The scheme provided an accuracy of < 1.3 pixels r.m.s. for MPI-9, MPI-10 and UC-1. We produced volume reconstructions by weighted backprojection³⁹. As each projection was combined into the volume, its grey-scale histogram was adjusted to compensate for uncontrolled variations in electron-beam exposure.

Signal restoration

We improved the signal-to-noise level in the reconstructed volume using nonlinear parametric signal estimation. A translation- and rotation-invariant tensor-wavelet transform was applied to serial two-dimensional volume slices perpendicular to the 0° tilt plane of the sample⁴⁰. Noise was reduced by discarding transform coefficients with values below a particular threshold. Image signal/noise ratio for the data presented here was improved by a factor of five, without significantly affecting the signal.

Segmentation

Structures were segmented from the reconstructed volume using a combination of manual and automatic methods applied to a series of two-dimensional slices. Each segmentation defined the boundaries of a volume of interest (VOI), a subset of the entire volume. We used two schemes to define the VOIs. For the presynaptic membrane and synaptic vesicles, which were heavily stained and had a simple geometry, a semi-automatic scheme was used in which the operator needed only to mark an anchor path on a single volume slice. We then automatically propagated this path perpendicular to the slice plane using a new, constrained grey-scale neighborhood-search scheme. For active zone material, which had a complex geometry and light to moderate stain, VOIs were defined by manually marking a closed path on a series of slices. The thickness of each slice for MPI-9 and MPI-10 was 0.52 nm (for example, Fig. 2c, d), and for UC-1 it was 1.2 nm. For all segmentation, the angular orientation of the slice plane was completely adjustable to maximize contrast boundary discrimination of the stained structure under study. The segmentation VOIs were slightly larger than the stained structures that they enclosed, to allow for accurate and complete isodensity surface calculations for surface renderings.

Surface rendering

To observe the stained structures within each VOI, a surface was calculated on the basis of a particular stain-density (grey) value. Initially, the isodensity value for each VOI was chosen to correspond to the 60% population value on the grey-scale cumulative distribution function; in some cases the value was subsequently adjusted slightly by the operator to correct for local inhomogeneities in stain density.

Received 14 September; accepted 24 November 2000.

1. Peters, A., Palay, S. L. & Webster, H. de F. *The Fine Structure of the Nervous System* 198–203 (Oxford, Oxford, 1991).
2. Katz, B. *The Release of Neural Transmitter Substances* (Thomas, Springfield, 1969).
3. Couteaux, R. & Pécot-Dechavassine, M. Vésicules synaptiques et poches au niveau des "zones actives" de la jonction neuromusculaire. *Compt. Rend.* **271**, 2346–2349 (1970).
4. Heuser, J. E. & Reese, T. S. Structural changes after transmitter release at the frog neuromuscular junction. *J. Cell Biol.* **88**, 564–580 (1981).
5. Palay, S. L. Synapses in the central nervous system. *J. Biophys. Biochem. Cytol.* **2** (Suppl.), 193–202 (1956).
6. Gray, E. G. Electron microscopy of presynaptic organelles of the spinal cord. *J. Anat.* **97**, 101–106 (1963).
7. Gray, E. G. Problems of interpreting the fine structure of vertebrate and invertebrate synapses. *Int. Rev. Gen. Exp. Zool.* **2**, 139–170 (1966).
8. Heuser, J. E. & Reese, T. S. in *Handbook of Physiology* Vol. 1, 261–294 (American Physiological Society, Bethesda, 1977).
9. Frank, J. *Electron Tomography: Three-Dimensional Imaging with the TEM* (Plenum, New York, 1992).
10. Radermacher, M. Three-dimensional reconstruction of single particles from random and nonrandom tilt series. *J. Electron Microsc. Tech.* **9**, 359–394 (1988).
11. Zhou, Z., Prasad, B., Jakana, J., Rixon, F. & Chiu, W. Protein subunit structures in the herpes simplex virus capsid from 400 kV spot-scan electron cryomicroscopy. *J. Mol. Biol.* **242**, 456–469 (1994).
12. Zwickl, P. et al. Primary structure of the thermoplasma proteasome and its implications for the structure, function, and evolution of the multicatalytic proteinase. *Biochemistry* **31**, 964–972 (1994).
13. Moritz, M. et al. Three-dimensional structural characterization of centrosomes from early *Drosophila* embryos. *J. Cell Biol.* **130**, 1149–1159 (1995).
14. Hoenger, A. & Aebi, U. 3-D reconstructions from ice-embedded and negatively stained biomacromolecular assemblies: A critical comparison. *J. Struct. Biol.* **117**, 99–116 (1996).
15. McEwen, B. F., Arena, J. T., Frank, J. & Rieder, C. L. Structure of the colcemid-treated PtK1 kinetochore outer plate as determined by high voltage electron microscopic tomography. *J. Cell Biol.*

- 120**, 301–312 (1993).
16. Perkins, G. et al. Electron tomography of neuronal mitochondria: three-dimensional structure and organization of cristae and membrane contacts. *J. Struct. Biol.* **119**, 260–272 (1997).
17. Ladinsky, M. S., Mastronarde, D. N., McIntosh, J. R., Howell, K. E. & Staehelin, L. A. Golgi structure in three dimensions: functional insights from the normal rat kidney cell. *J. Cell Biol.* **144**, 1135–1149 (1999).
18. Lenzi, D., Runyeon, J. W., Crum, J., Ellisman, M. H. & Roberts, W. M. Synaptic vesicle populations in saccular hair cells reconstructed by electron tomography. *J. Neurosci.* **19**, 119–132 (1999).
19. Heuser, J. E., Reese, T. S. & Landis, D. M. D. Functional changes in frog neuromuscular junctions studied with freeze-fracture. *J. Neurocytol.* **3**, 109–131 (1974).
20. Robitaille, R., Alder, E. M. & Charlton, M. P. Strategic location of calcium channels at transmitter release sites of frog neuromuscular synapses. *Neuron* **5**, 773–779 (1990).
21. Stanley, E. F. The calcium channel and the organization of the presynaptic transmitter release face. *Trends Neurosci.* **20**, 404–409 (1997).
22. Catterall, W. A. Structure and function of neuronal Ca²⁺ channels and their role in neurotransmitter release. *Neuron* **24**, 307–323 (1998).
23. McMahan, U. J. & Slater, C. R. The influence of basal lamina on the accumulation of acetylcholine receptors at synaptic sites in regenerating muscle. *J. Cell Biol.* **98**, 1453–1473 (1984).
24. Colledge, M. & Froehner, S. C. To muster a cluster: anchoring neurotransmitter receptors at synapses. *Proc. Natl Acad. Sci. USA* **95**, 3341–3345 (1998).
25. Robitaille, R., Garcia, M. L., Kaczorowski, G. J. & Charlton, M. P. Functional colocalization of calcium and calcium-gated potassium channels in control of transmitter release. *Neuron* **11**, 645–655 (1993).
26. Cohen, M. W., Hoffstrom, B. G. & DeSimone, D. W. Active zones on motor nerve terminals contain $\alpha 3\beta 1$ integrin. *J. Neurosci.* **20**, 4912–4921 (2000).
27. Weber, T. et al. SNAREpins: minimal machinery for membrane fusion. *Cell* **92**, 759–772 (1998).
28. Hazuka, C. D., Foletti, D. L. & Scheller, R. H. in *Neurotransmitter Release* (ed. Bellen, H. J.) 81–125 (Oxford Univ. Press, 1999).
29. Jahn, R. & Südhof, T. C. Membrane fusion and exocytosis. *Annu. Rev. Biochem.* **68**, 863–911 (1999).
30. Broadie, K., Bellen, H. K., DiAntonio, J., Littleton, J. T. & Schwarz, T. L. Absence of synaptotagmin disrupts excitation-secretion coupling during synaptic transmission. *Proc. Natl Acad. Sci. USA* **91**, 10727–10731 (1994).
31. Pfeffer, S. R. Transport-vesicle targeting: tethers before SNAREs. *Nature Cell Biol.* **1**, E17–E22 (1999).
32. Sunderland, W. J., Son, Y.-J., Miner, J. H., Sanes, J. R. & Carlson, S. S. The presynaptic calcium channel is part of a transmembrane complex linking a synaptic laminin ($\alpha 4\beta 2\gamma 1$) with non-erythroid spectrin. *J. Neurosci.* **20**, 1009–1019 (2000).
33. Martin, P. T., Kaufman, S. J., Kamer, R. H. & Sanes, J. R. Synaptic integrins in developing, adult, and mutant muscle: selective association of $\alpha 1$, $\alpha 7A$, $\alpha 7B$ integrins in the neuromuscular junction. *Dev. Biol.* **174**, 125–139 (1996).
34. Bewick, G. S., Young, C. & Slater, C. R. Spatial relationships of utrophin, dystrophin, β -dystroglycan, and β -spectrin to acetylcholine receptor clusters during postnatal maturation of the rat neuromuscular junction. *J. Neurocytol.* **25**, 367–369 (1996).
35. Ress, D., Harlow, M., Schwarz, M., Marshall, R. M. & McMahan, U. J. Automatic acquisition of fiducial markers and alignment of images in tilt series for electron tomography. *J. Electron Microsc.* **48**, 277–287 (1999).
36. Dierksen, K., Typke, D., Hegerl, R. & Baumeister, W. Towards automatic electron tomography. *Ultramicroscopy* **49**, 109–120 (1992).
37. Dierksen, K. et al. Three dimensional structure of lipid vesicles embedded in vitreous ice and investigated by automatic electron tomography. *J. Biophys.* **68**, 1416–1422 (1995).
38. Braunfeld, M., Koster, A., Sedat, J. & Agard, D. Cryo automated electron tomography: towards high-resolution reconstructions of plastic-embedded structures. *J. Microsc.* **174**, 75–84 (1994).
39. Radermacher, M. in *Electron Tomography: Three-Dimensional Imaging with the TEM* (ed. Frank, J.) 91–115 (Plenum, New York, 1992).
40. Stoschek, A. & Hegerl, R. Denoising of electron tomographic reconstructions using multiscale transformations. *J. Struct. Biol.* **120**, 257–265 (1997).
41. Wang, X. et al. Aczonin, a 550-kD putative scaffolding protein of presynaptic active zones, shares homology regions with Rim and Bassoon and binds profilin. *J. Cell Biol.* **147**, 151–162 (1999).

Supplementary information is available on Nature's World-Wide Web site (<http://www.nature.com>) or as paper copy from the London editorial office of Nature.

Acknowledgements

We are grateful to W. Baumeister and members of the Department of Structural Biology at the Max-Planck Institute for Biochemistry in Martinsried, Germany, for use of their CM 200 electron microscope; A. Koster participated in the data collection for MPI-9 and MPI-10. We are also grateful to D. Agard and members of his laboratory in the Department of Biochemistry and Biophysics at the University of California San Francisco for use of the Philips EM 430; M. Braunfeld participated in the data collection for UC-1. T. Schwarz at Harvard Medical School provided comments on the manuscript, and B. Colyear at Stanford University made the schematic illustrations. This work was supported by grants from the NIH and the Deutsche Forschungsgemeinschaft, and by the M. A. Antelman Fund.

Correspondence and requests for materials should be addressed to U.J.M. (e-mail: ujmcmahan@stanford.edu).